Colloid Polym Sci 278:202–210 (2000)

ORIGINAL CONTRIBUTION

T. Okubo
A. Tsuchida
S. Takahashi
K. Taguchi
M. Ishikawa

Kinetics of colloidal alloy crystallization of binary mixtures of monodispersed polystyrene and/or colloidal silica spheres having different sizes and densities in microgravity using aircraft

Received: 19 July 1999
Accepted in revised form: 1 September 1999

T. Okubo (✉) · A. Tsuchida
S. Takahashi · K. Taguchi
Department of Applied Chemistry
Gifu University, Yanagido 1-1
Gifu 501-1193, Japan
e-mail: okubotsu@apchem.gifu-u.ac.jp
Fax: +81-58-2932628

M. Ishikawa
Mitsubishi Research Institute Inc.
2-3-6 Otemachi, Chiyoda-ku,
Tokyo 100-0004, Japan

Abstract Crystal growth rates in colloidal alloy crystallization of binary mixtures of monodispersed polystyrene and/or silica spheres having different sizes and densities are studied in microgravity by parabolic flights of an aircraft. The crystal growth rates are obtained by time-resolved reflection spectroscopy with a continuous circulating-type stopped-flow-cell system. The growth rates of alloy crystallization increase substantially in microgravity up to about 1.7 times those in normal gravity, which is in contrast to the retarding microgravity effect on the crystallization of single-component spheres. The disappearance of the segregation effect in microgravity is the main cause for the enhancing effect. The absence of convection of the suspension and the lack of downward sedimentation of colloidal spheres are also important.

Key words Colloidal alloy crystals · Crystal growth kinetics · Microgravity effect · Reflection spectroscopy · Segregation

Introduction

As far as the authors know, the sedimentation effect for colloidal crystals in normal gravity was first discussed quantitatively by Crandall and Williams [1] and later by Furusawa and Tomotsu [2]. We have studied microscopic and spectroscopic features of colloidal gases, liquids and crystals at sedimentation equilibrium [3–8]. Furthermore, sedimentation velocities and the diffusion equilibria of colloidal gases and crystals have been studied [9, 10]. The importance of gravity is now clear for some colloidal suspension properties. The elastic moduli of colloidal crystals are very low, of the order of 10^{-2}–10^{3} Pa, compared with those of metals, 10^{10} (lead) to 10^{12} Pa [1, 2, 4, 11, 12]. Thus, the colloidal structure is distorted greatly and can be broken by shearing force and elevated pressure. Even weak external fields, such as gravitational or centrifugal fields, can distort the structure of colloidal crystals when the density of the colloidal particles is different from that of the solvent. In a suspension of mixed spheres with two different diameters, segregation occurs because of the gravitational field, and the larger and smaller spheres are separated into the upper and lower parts, respectively. Quite recently Zhu et al. [13] reported the microgravity effect on the morphology of colloidal crystals formed in microgravity using the Space Shuttle Columbia.

Recently, we have reported kinetics studies of the colloidal crystallization of silica spheres in highly diluted and exhaustively deionized states [14, 15]. In these experiments the crystal growth rates were measured by static light scattering and dynamic light scattering and also by reflection spectroscopy (RS). RS is a very powerful method to study the kinetics of colloidal crystallization [11, 16]. The crystal growth process was explained beautifully by the classical diffusion theory of crystallization, though the restricted diffusion of the reacting spheres as in fused metal systems was taken into account. The crystal growth rates ranged from 1 to 27 μm/s and increased substantially as the sphere concentration increased. We have also studied nucleation and growth processes in the colloidal crystallization of silica spheres (specific gravity = 2.2, diameter = 110 nm) in microgravity achieved by the

parabolic flights of an aircraft [17]. The crystal growth rates of face-centered cubic lattices decreased in microgravity (0G) by 25–30% compared with those in normal gravity (1G). One of the main reasons for the retardation was attributed to the fact that the downward diffusion of spheres, which may enhance the inter sphere collisions, disappears at 0 G. The absence of convection of the suspension at 0 G was also important.

For binary mixtures of monodispersed colloidal spheres alloy structures have been studied by Hachisu and Yoshimura [9, 10]. The superlattice structures observed hitherto are $A1B_2$, $NaZn_{13}$, $CaCu_5$, $MgCu_2$, and AB_4 types. These structures have been analyzed successfully based on the hard-sphere model. The structure type was determined by the ratio of the effective diameters, including the Debye screening length of the constituent spheres. Ionic groups on the colloidal surfaces leave their counterions in the suspension, and these excess charges accumulate near the surface forming an electrical double layer. The double layer consists of two regions, an inner region composed of adsorbed counterions (the Helmholtz layer) and a diffuse region containing the remainder of the excess counterions (Gouy–Chapman layer). The counterions in the diffuse region are distributed according to a balance between their thermal motion and the forces of electrical attraction with the colloidal spheres. The thickness of the electrical double layer is approximated by the Debye screening length, D_1,

$$D_1 = (4\pi e^2 n/\varepsilon k_B T) \ , \qquad (1)$$

where e is the electronic charge, ε is the dielectric constant of the solvent, k_B is the Boltzmann constant, and n is the concentration of free-state cations and anions in suspension and is given by $n = n_c + n_s + n_o$, where n_c is the concentration (number of ions per cubic centimeter) of diffusible counterions, n_s is the concentration of foreign salt, and n_o is the concentration of both H^+ and OH^- from the dissociation of water. In order to estimate n_c the fraction of free counterions (β) must be known, since most counterions are bound tightly with the ions on the colloidal surface. Note that the maximum observed and calculated values of D_1 are both very long: about 1 μm in water.

We should note here that the segregation effect, i.e., large spheres are segregated upward and small ones downward in normal gravity, is significant for binary mixtures of colloidal spheres. We have studied the two-dimensional structures of binary colloidal mixtures of different sizes and densities in sedimentation equilibrium [3, 18, 19]: the segregation effect was substantial. In this work crystal growth rates in the colloidal alloy crystallization of binary mixtures of monodispersed polystyrene and/or silica colloidal spheres were studied for the first time in microgravity achieved by the parabolic flights of an aircraft.

Experimental

Materials

D1W52 and D1B76 were monodispersed polystyrene spheres purchased from Dow Chemicals Co. Monodispersed colloidal silica spheres of CS-91 and CS-121 were kindly donated by Catalysts & Chemicals Ind. Co. (Tokyo). The diameter (d), the standard deviation (δ) from the mean diameter, the polydispersity index (δ/d), and the specific gravity are listed in Table 1. The values of d and δ were determined with a transmission electron microscope (JEOL, Tokyo, type JEM-2000FX). The surface charge densities of the spheres were determined by conductometric titration with a Wayne–Kerr autobalance precision bridge, model B331, mark II (Bogner Regis, UK) or a Horiba conductivity meter, model DS-14 (Kyoto) [20, 21]. All these spheres have strongly acidic and weakly acidic groups. The strongly acidic groups are the sulfate groups originating from the initiator added in the polymerization process and a part of the silanol groups located at the sphere surface for the polystyrene and silica spheres, respectively. The weakly acidic groups are carboxylic acid groups and most of the silanol groups. The sphere samples were purified carefully several times using an ultrafiltration cell (model 202, membrane: Diaflo XM, Amicon Co., Lexington, Ky., USA) and then treated with a mixed bed of cation- and anion-exchange resins [Bio-Rad, AG501-X8 (D), 20–50 mesh] for more than 4 years. The sample suspensions set in the cell were deionized at least 15 h before measurements with a flow rate of 3 ml/min. The water used for the preparation of the sample suspensions was obtained from a Milli-Q water system (Milli-RO Plus and Milli-Q Plus, Millipore, Bedford, Mass. USA). All the experiments were performed at 25 °C.

Reflection spectroscopy

The cell system used, which was the same as the one reported previously [17], consists of a quartz observation cell ($40 \times 10 \times 2$ mm), a column of cation- and anion-exchange resins (Bio-Rad), and a peristaltic pump (Masterflex 7524-10, Ill., USA). The pump circulates the colloidal suspensions first to the resin column and then to the observation cell in order to deionize the suspension continuously. The flow rate was usually 3 ml/min as previously described. The rate was increased to 9 ml/min before the measurements were taken. A light beam from a halogen lamp (Hayashi LA-150SX, Tokyo) hits the cell wall through a Y-type optical fiber cable and the reflection spectra are taken on a photonic multichannel analyzer (PMA-50, Hamamatsu Photonics, Hamamatsu). When the colloidal suspension is passed into the narrow observation cell, the crystals are melted away by the shear flow. After stopping the flow, crystallization starts. The crystal growth process was followed from the growth of the Bragg reflection peaks. In our experimental conditions the suspension in the flow cell (2 mm path length) was transparent. Thus, the RS in our experiments affords information on the crystal growth processes over the whole depth of the suspension in the cell. The duration of the microgravity environment was 22 s. Within 20 s 200

Table 1 Properties of the colloidal spheres used

Sphere	d (nm)	δ (nm)	δ/d	Specific gravity	Charge density (μm/cm^2)	
					strong acid	weak acid
D1W52	88	6.2	0.07	1.05	1.14	1.7
D1B76	109	3	0.028	1.05	2.1	0.71
CS-91	110	4.5	0.041	2.2	0.48	–
CS-121	136	10.9	0.08	2.2	0.40	–

time-resolved reflection spectra were taken. The measurements started 0.5 s before the circulation of the colloidal suspension was stopped. Close-up observation of the flow cell was also made with a charge-coupled device (CCD) camera (Elmo EM-102T, Nagoya).

A Mitsubishi MU-300 jet aircraft was used for the microgravity experiments. Three types of measurements were made for each flight:

1. On the ground in a plane before flight at 1 G.
2. During flight to the test area at 1 G.
3. In microgravity at 0 G. Measurements 1 and 2 were made to obtain reference data at 1 G and to examine the vibrational effects of the airplane on the kinetic parameters, respectively.

Results and discussion

Kinetics of colloidal alloy crystallization in normal gravity

According to the effective hard-sphere model [22–28], which is a simple but very convenient assumption for colloidal crystallization, crystal-like ordering of the single component spheres occurs when the effective diameter (d_{eff}) of the spheres including a Debye screening length is close to or larger than the intersphere distance (D), i.e., $d_{\mathrm{eff}} = [\text{diameter } (d) + 2 \times D_1] > D$. At $\phi = 0.005$ of the CS-91 spheres for example, d_{eff} was calculated to be 800 nm. Here, the fraction of free-state counterions (β) was assumed to be 0.1. d_{eff} was larger than the intersphere distance, 580 nm, which was calculated assuming the sphere distribution of a simple cubic lattice. This supports the validity of the effective hard-sphere model.

The mean intersphere distance (D_0), when two different spheres were distributed in the substitutional solid solution (sss) or body-centered cubic, is calculated using Eq. (2) [3, 18],

$$D_0 = \left[\left(\phi_1/0.68\, d_1^3\right) + \left(\phi_2/0.68\, d_2^3\right)\right]^{-1/3} , \qquad (2)$$

Table 2 Secondary peak wavelengths (λ_p) and final crystal sizes (L) at 1 and 0 G at 25 °C. The total sphere concentrations in the mixtures were always 0.005 in volume fraction

			ϕ_{D1W52}:ϕ_{D1B76}				
			1:0	3:1	1:1	1:3	0:1
λ_p (nm)	Obs.	1 G	–	561(s)[a]	578(s)	603(s)	631(s)
			–	649(v)[a]	664(v)	699(v)	719(v)
		0 G	–	566(s)	582(s)	606(s)	630(s)
			–	646(v)	666(v)	696(v)	721(v)
	Calc.		–	514	539	570	627
L (mm)	Obs.	1 G	–	0.13	0.26	0.13	0.13
		0 G	–	0.13	0.13	0.13	0.13
			ϕ_{CS-91}:ϕ_{CS-121}				
λ_p (nm)	Obs.	1 G	645	664	693	720	750
			736	761	791	825	
		0 G	646	669	698	722	753
			737	763	792	823	
	Calc.		633	642	673	712	783
L (mm)	Obs.	1 G	0.13	0.13	0.13	0.26	0.13
		0 G	0.13	0.13	0.26	0.26	0.13
			ϕ_{D1B76}:ϕ_{CS-91}				
λ_p (nm)	Obs.	1 G	631	663	683	643	645
			719	758	780	735	736
		0 G	630	663	686	645	646
			721	761	783	738	737
	Calc.		627	611	613	595	633
L (mm)	Obs.	1 G	0.13	0.13	0.26	0.26	0.13
		0 G	0.13	0.13	0.26	0.26	0.13
			ϕ_{D1B76}:ϕ_{CS-121}				
λ_p (nm)	Obs.	1 G	631	660	688	734	750
			719	756	790	839	
		0 G	630	660	691	735	753
			721	758	790	843	
	Calc.		627	637	669	709	783
L (mm)	Obs.	1 G	0.13	0.26	0.13	–	0.13
		0 G	0.13	0.26	0.13	–	0.13

[a](s) and (v) indicate sharp and vague peaks, respectively

where ϕ_1 and ϕ_2 are the volume fractions of spheres 1 and 2, respectively, and d_1 and d_2 are the diameters of each sphere. All the peak wavelengths measured at 1 and 0 G are shown in Table 2; the calculated peak wavelengths from Eq. (2) are also listed. Agreement between the observed and calculated values is satisfactory when the experimental errors are taken into account. The observed values suggest the formation of alloy structures of sss type and/or the superlattices [3, 18]. The peak wavelengths observed for the single-sphere systems also agreed satisfactorily with the corresponding calculation.

The final sizes of the colloidal crystals formed were estimated from the video pictures taken by the CCD camera. The results are listed in Table 2. Mixing of two different systems often produced larger single crystals. Generally, the size of the colloidal single crystals increased as the sphere concentration decreased, and the largest crystals were formed at sphere concentrations slightly higher than the critical sphere concentration of melting [29]. Thus, an increase in crystal size for the binary mixtures means that the suspension state is close to the critical condition of melting.

The reflection spectra in the course of crystallization of a D1B76 + CS-91 (1:3) mixture ($\phi_{\text{total}} = 0.005$) in normal gravity form 0 to 18.7 s after stopping the flow are shown in Fig. 1. Two reflection peaks appeared at 643 and 735 nm, though the latter was rather vague. The sharp peak was assigned to the secondary peak, because the secondary peak wavelength was calculated from the sphere concentration to be 595 nm. Assignment of the vague peak at 735 nm has not been achieved yet. A slight blue-shift in the peaks was observed in the course of crystallization, which suggests the crystals become denser in the growth process.

The time dependence of the peak intensities in normal gravity is shown in Fig. 2 for the blue-side peak in Fig. 1. As is clear in the figure, crystal growth was almost complete within about 15 s of stopping the flow. The rates of crystallization, v, should be evaluated from the slope of the time dependencies of the cube root of the peak intensities [17]; however, preliminary analyses of the data, where the cube roots of the intensities are plotted against time, gave large uncertainties. Thus, the rate coefficient, k, was introduced instead of v in this work. The k values were obtained as the reciprocal period where the initial linear line in the peak intensities intersects two horizontal lines giving initial and final intensities at $t = t_i$ and $t = t_f$, respectively, i.e., $k = 1/(t_f - t_i)$. The t_i value corresponds to the induction time for crystallization.

Four combinations of different sphere mixtures were examined with five different mixing ratios for each combination in this work. The D1W52 + D1B76 system consists of small (88 nm) and large (109 nm) polystyrene spheres with the same density. The CS-91 + CS-121 system is a mixture of small (110 nm) and large (136 nm) silica spheres with the same density. The

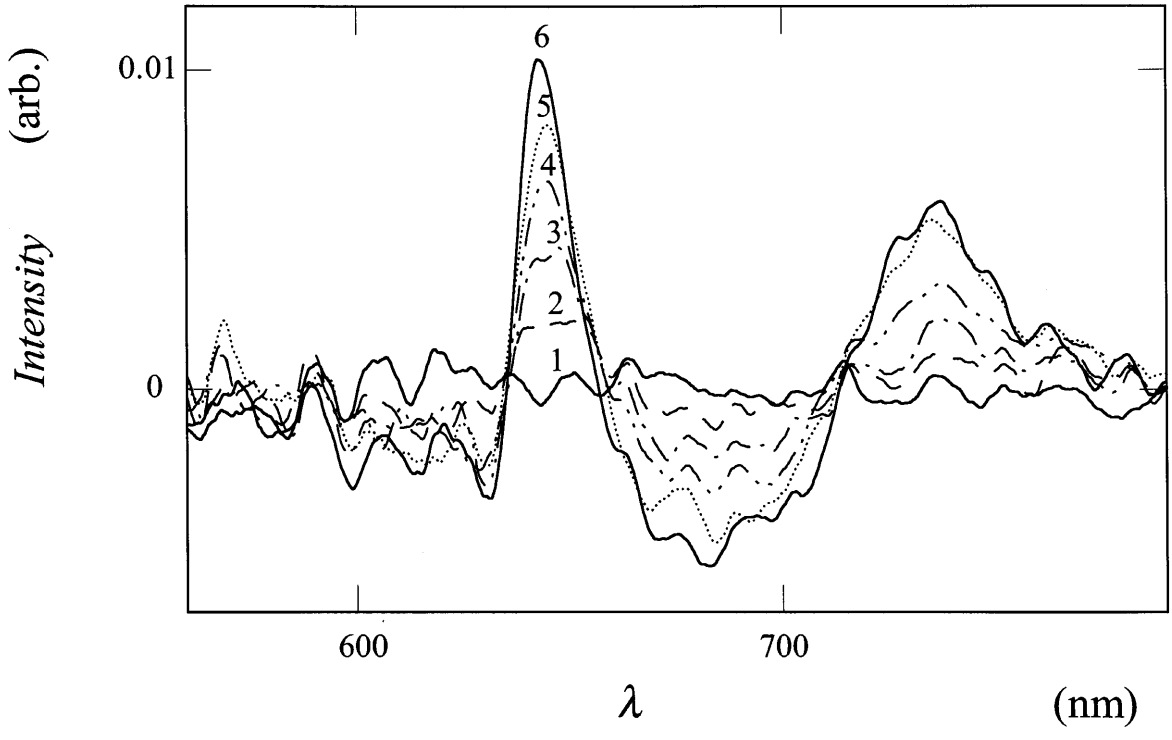

Fig. 1 Reflection spectra of colloidal crystals of D1B76 + CS-91 (1:3) spheres at 1 G, 25 °C, $\phi_{\text{total}} = 0.005$. Curve *1*, $t = 0$ s; Curve *2*, $t = 1.5$ s; Curve *3*, $t = 3.1$ s; Curve *4*, $t = 4.5$ s; Curve *5*, $t = 10$ s; Curve *6*, $t = 18.7$ s

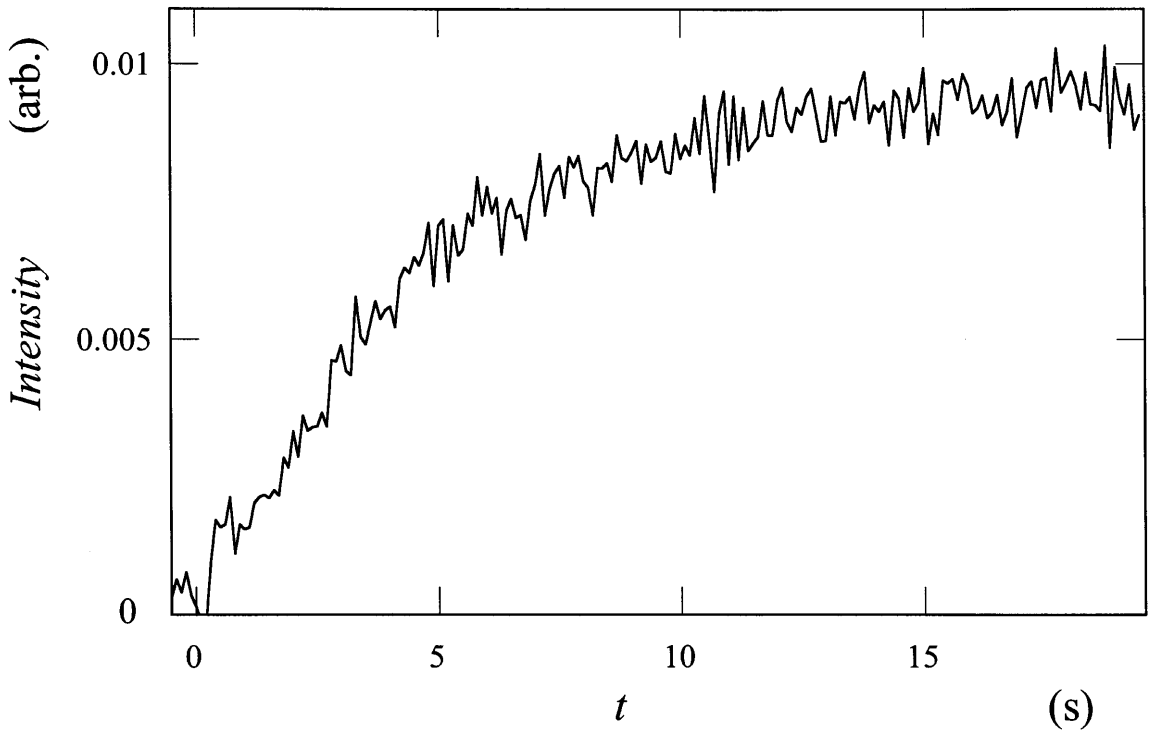

Fig. 2 Reflection intensities in the course of colloidal crystallization of D1B76 + CS-91 (1:3) spheres at 1 G, 25 °C; $\phi_{total} = 0.005$

Fig. 3 Rate coefficients as a function of sphere volume fraction in D1W52 + D1B76 mixtures at 0 G (○) and 1 G (×) at 25 °C; $\phi_{total} = 0.005$. x denotes the volume fraction of D1B76 spheres in the mixture

D1B76 + CS-91 system is a mixture of less dense polystyrene (specific gravity = 1.05) and dense silica (2.2) spheres with the same diameter. The D1B76 + CS-121 system is a combination of small, less dense (109 nm diameter and 1.05 specific gravity) and large, dense (136 nm and 2.2) spheres. It should be noted here that the alloy structure for the mixture of D1B76 and D1C25

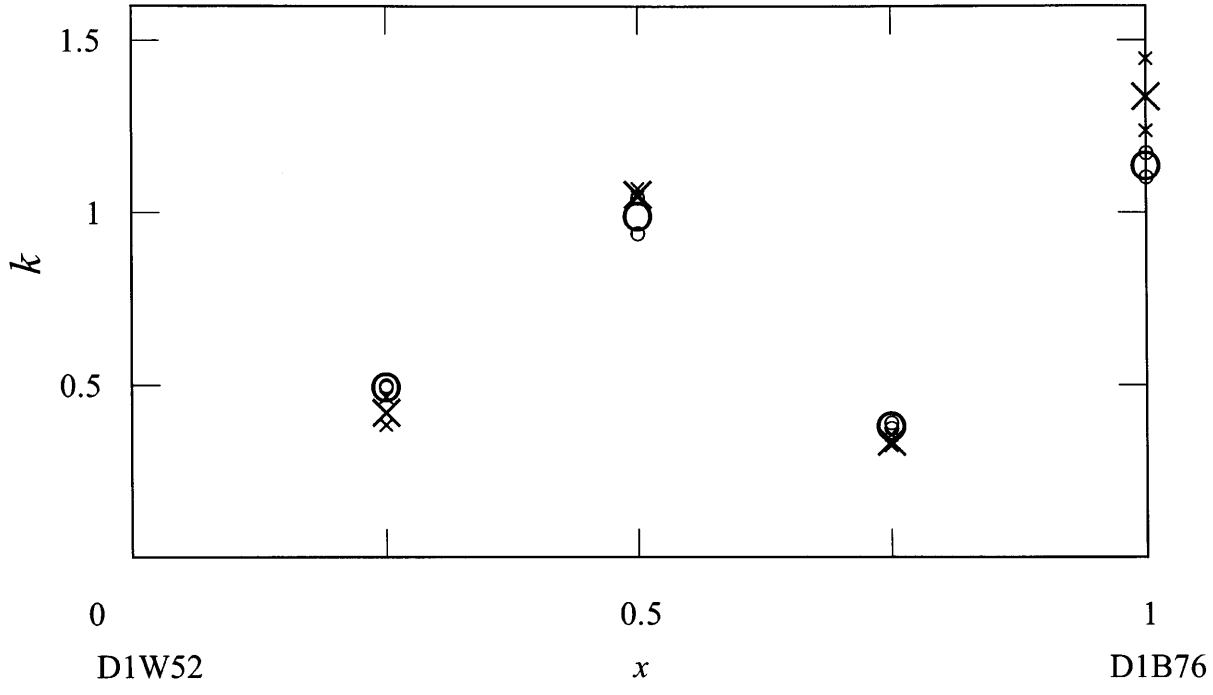

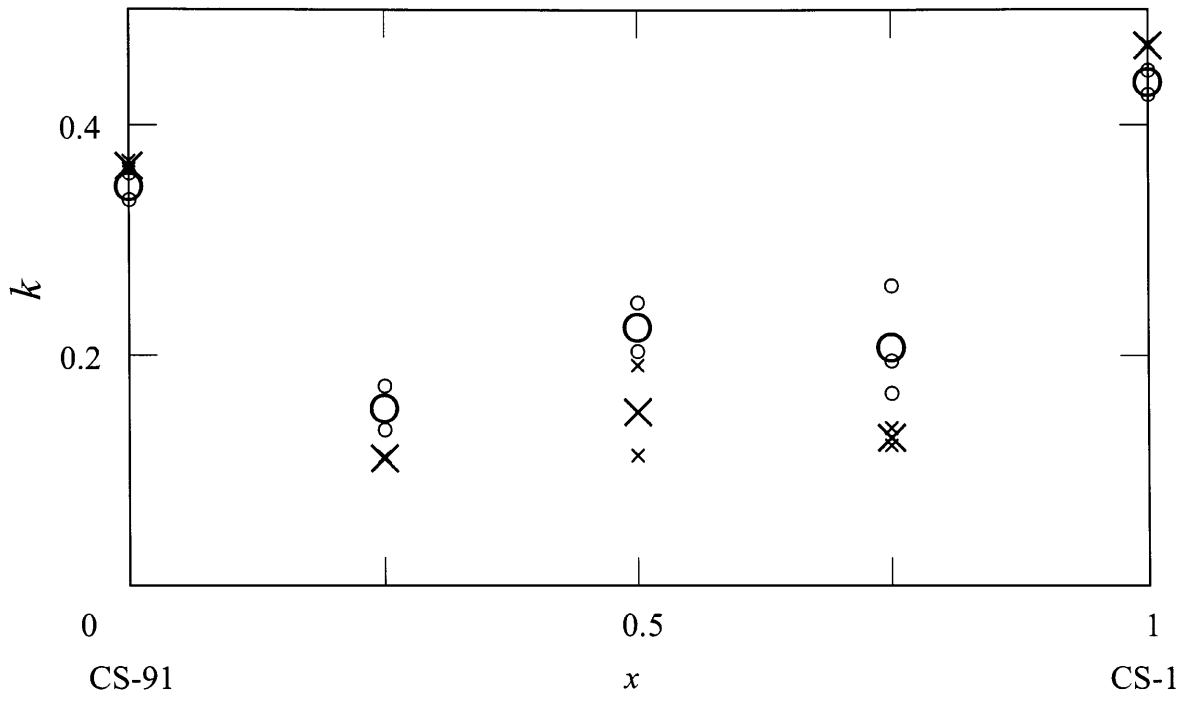

Fig. 4 Rate coefficients as a function of sphere volume fraction in CS-91 + CS-121 mixtures at 0 G (○) and 1 G (×) at 25 °C; ϕ_{total} = 0.005. x denotes the volume fraction of CS-121 spheres in the mixture

Fig. 5 Rate coefficients as a function of sphere volume fraction in D1B76 + CS-91 mixtures at 0 G (○) and 1 G (×) at 25 °C; ϕ_{total} = 0.005. x denotes the volume fraction of CS-91 spheres in the mixture

(85 nm) spheres will sss-type lattices. The $MgCu_2$-type superlattices detected previously [3] were not observed at any mixing ratios examined using this RS. The crosses in Figs. 3–6 (large marks are the average values) show the observed rate coefficients for each mixture as a function of sphere volume fraction in normal gravity. For all the binary mixture systems the rate coefficients were small compared with those of single-component systems. It is

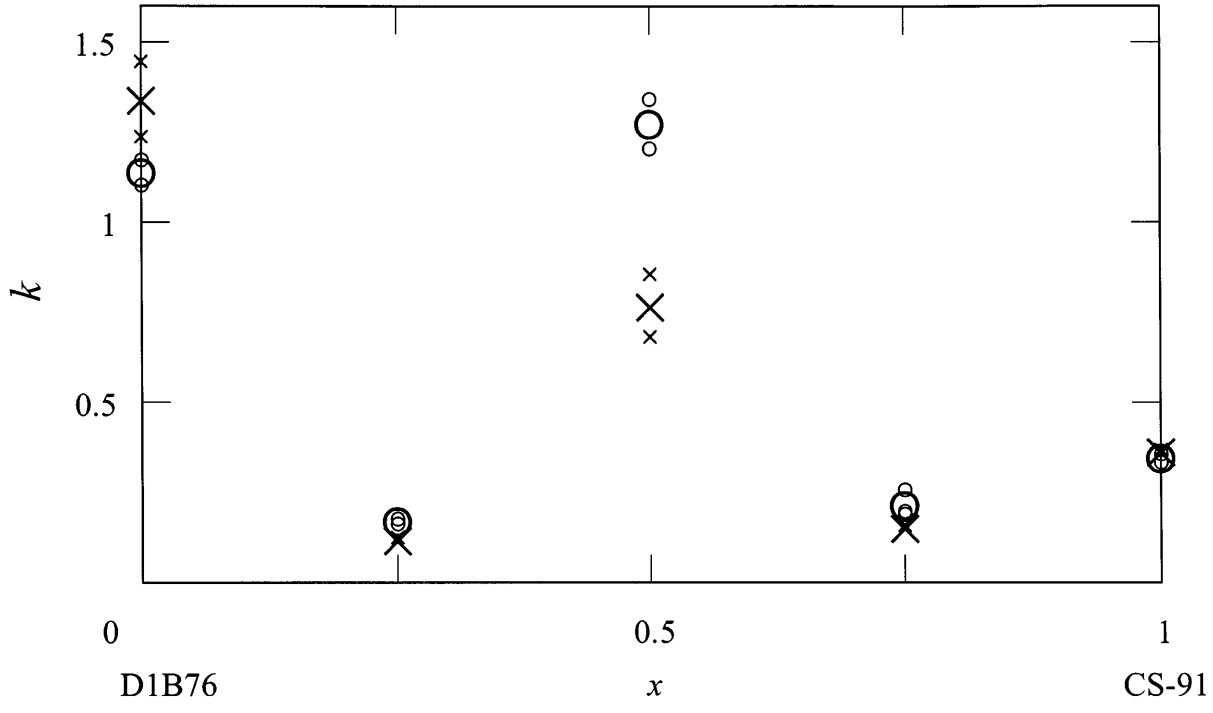

interesting to note that the k values of the 1:1 mixture systems are not so small compared with those of mixtures with 3:1 and 1:3 ratios. These experimental observations must be strongly correlated to the factor of how the extent of the dead volume decreases by mixing spheres having various sizes and volume fractions in the packing model [30–36].

Kinetics of colloidal alloy crystallization in microgravity

The reflection spectra of the D1B76 + CS-91 (1:3) mixture (ϕ_{total} = 0.005) in the course of crystallization in microgravity from 0 to 19.4 s after stopping the flow are shown in Fig. 7. The peak wavelengths and the crystal sizes obtained in the microgravity experiments are compiled in Table 2. No significant differences in the spectral profiles are observed between those in normal gravity and those in microgravity. This suggests that the crystallization mechanism is the same between 0 and 1 G. The k values at 0 G were also quite sensitive to the mixing ratio and those of 1:1 mixtures were large compared with the other mixing ratios of 1:3 and 3:1.

The rate coefficient ratios k_{0G}/k_{1G} are shown in Fig. 8. Clearly, large k_{0G}/k_{1G} values were obtained for CS-91 + CS-121 and D1B76 + CS-91 mixtures. The

Fig. 6 Rate coefficients as a function of sphere volume fraction in D1B76 + CS-121 mixtures at 0 G (○) and 1 G (×) at 25 °C; ϕ_{total} = 0.005. x denotes the volume fraction of CS-121 spheres in the mixture

Fig. 7 Reflection spectra of colloidal crystals of D1B76 + CS-91 (1:3) spheres at 0 G, 25 °C, ϕ_{total} = 0.005. Curve *1*, t = 0 s; Curve *2*, t = 1.2 s; Curve *3*, t = 2.9 s; Curve *4*, t = 3.6 s; Curve *5*, t = 8.1 s; Curve *6*, t = 19.4 s

former system is a combination of the same sphere densities but different sphere sizes and the latter system is a mixture of spheres having the same sizes but different specific gravities. In normal gravity small spheres sediment faster than large ones and heavy spheres drop faster than light ones. The maximum value of k_{0G}/k_{1G} was about 1.7, and the microgravity effect was quite large. In microgravity, the segregation effect should disappear and totally homogeneous mixing must occur, which leads to faster alloy structure formation. The absence of convection must also be quite favorable for alloy distribution. This striking acceleration effect of microgravity in the alloy crystallization strongly suggests that the alloy ordering of colloidal spheres is explainable by the packing model, i.e., the alloy structure is determined by the maximum packing density for a given ratio of the sphere diameters including the thickness of the electrical double layers.

For the binary systems of D1B76 + CS-121 and D1W52 + D1B76, k_{0G}/k_{1G} was close to unity. The former system is a combination of small, less dense and large, dense spheres, where the segregation effects from the size and density differences will be canceled by each other even at 1 G. For the mixture of D1W52 + D1B76, the densities of the spheres (1.05) are close to that of water, and, furthermore, both spheres are so small that

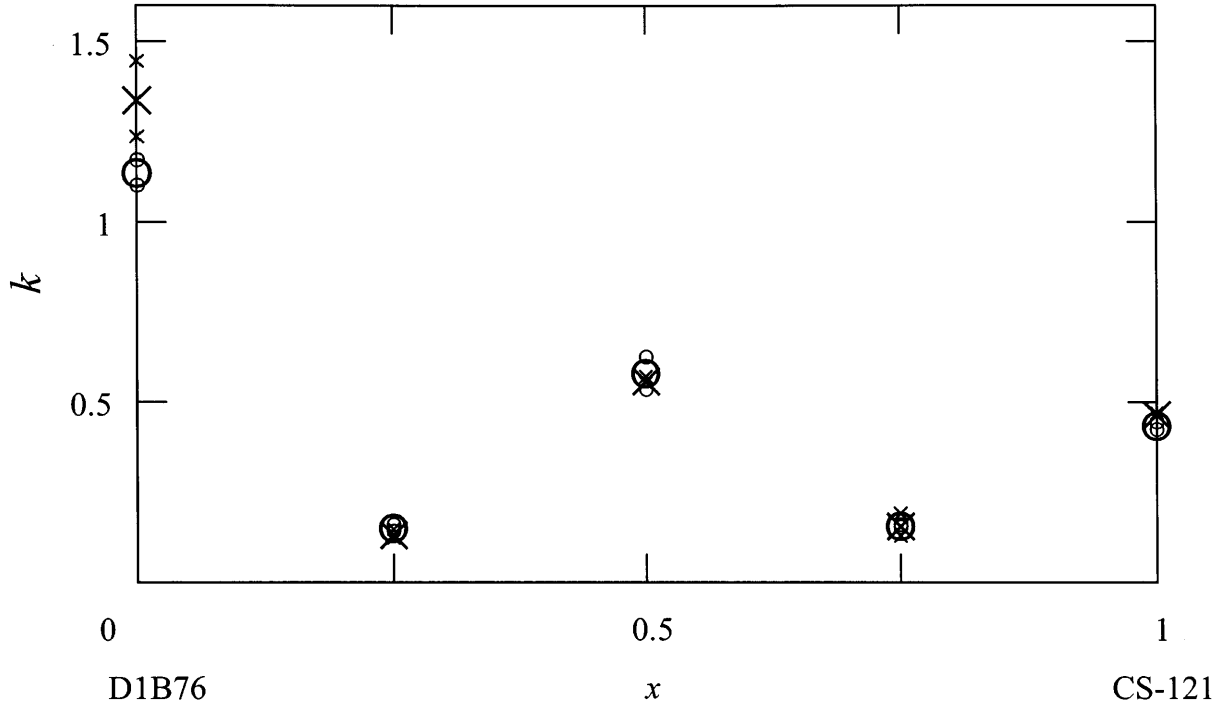

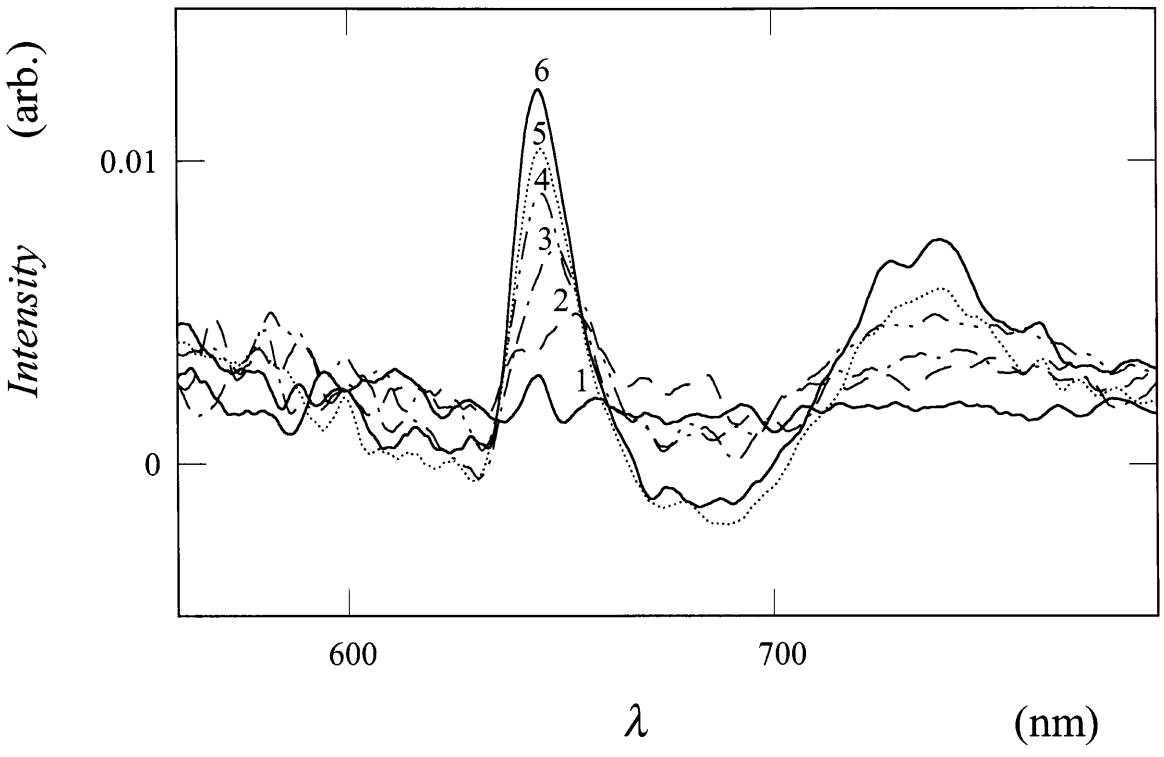

the effective sizes including electrical double layers are quite similar to each other. These are the main reasons why the microgravity effect was not so significant. It should be further noted that the acceleration effect in microgravity was largest at $x = 0.5$.

Fig. 8 Rate coefficient ratios as a function of sphere volume fraction in $[D1W52]_{1-x}$ + $[D1B76]_x$ (○), $[CS\text{-}91]_{1-x}$ + $[CS\text{-}121]_x$ (×), $[D1B76]_{1-x}$ + $[CS\text{-}91]_x$ (△) and $[D1B76]_{1-x}$ + $[CS\text{-}121]_x$ (□) mixtures at 25 °C. $\phi_{total} = 0.005$

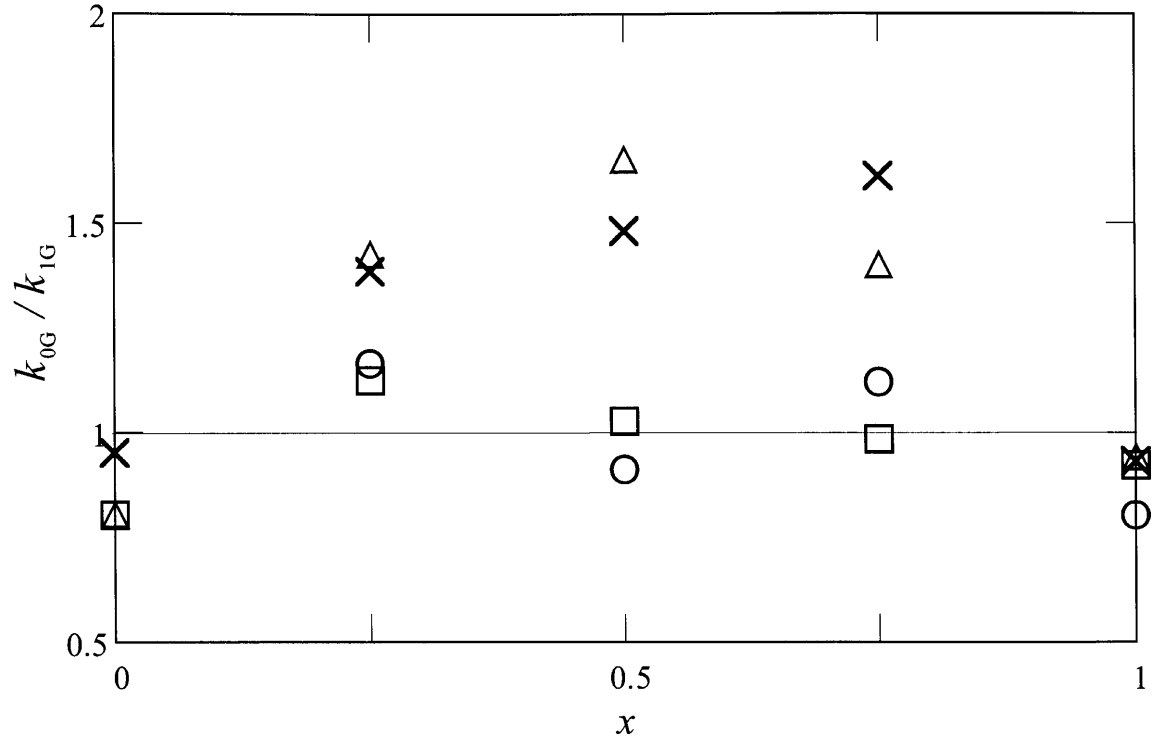

The values of k_{0G}/k_{1G} for the single-component systems were always less than unity, i.e., the colloidal crystallization rates were retarded in microgravity. As discussed in a previous work [17], one of the main causes is the lack of the extra downward diffusion of spheres, which enhances intersphere collisions, in microgravity. It is also highly plausible that the absence of convection in microgravity is also not favorable for the crystallization of single-component spheres.

Acknowledgements The authors are grateful to the National Space Development Agency of Japan and the Japan Space Forum for their financial support. M. Komatsu and M. Hirai of Catalysts & Chemicals Ind. Co. (Tokyo) are gratefully acknowledged for providing the colloidal silica sphere samples. Diamond Air Service Co. is also acknowledged for carrying out the parabolic flights. The quartz glass flow cell was made by Nakamura Glass Co. (Kyoto). The Ministry of Education, Science, Sports, and Culture is thanked for Grants-in-Aid for Scientific Research on Priority Areas (A) (11167241) and for Scientific Research (B) (11450367).

References

1. Crandall RS, Williams R (1977) Science 198:293
2. Furusawa K, Tomotsu N (1983) J Colloid Interface Sci 93:504
3. Okubo T (1990) J Chem Phys 93:8276
4. Okubo T (1988) Acc Chem Res 21:281
5. Okubo T (1989) J Chem Soc Faraday Trans 1 85:455
6. Okubo T (1990) J Chem Soc Faraday Trans 86:151
7. Okubo T (1994) J Phys Chem 98:1472
8. Okubo T (1995) J Chem Phys 102:7721
9. Hachisu S, Yoshimura S (1980) Nature 283:188
10. Yoshimura S, Hachisu S (1983) Prog Colloid Polym Sci 68:59
11. Okubo T (1994) In: Schmitz KS (ed) Macroion characterization. From dilute solutions to complex fluids. ACS Symposium Series 548. American Chemical Society, Washington, D.C., pp 346–380
12. Okubo T (1987) J Chem Phys 86:2394–2399
13. Zhu J, Li M, Rogers R, Meyer W, Ottewill RH, STS-73 Space Shuttle Crew, Russel WB, Chaik PM (1997) Nature 387:883
14. Okubo T, Okada S, Tsuchida A (1987) J Colloid Interface Sci 189:337–347
15. Okubo T, Okada S (1998) J Colloid Interface Sci 204:198–204
16. Okubo T (1988) J Chem Soc Faraday Trans 1 84:1163–1169
17. Okubo T, Tsuchida A, Okuda T, Fujitsuna K, Ishikawa M, Morita T, Tada T (1999) Colloids Surf 153:515–524
18. Okubo T, Fujita H (1996) Colloid Polym Sci 274:368–374
19. Okubo T (1987) J Chem Phys 87:5528–5533
20. Okubo T (1993) Colloid Polym Sci 271:190–196
21. Okubo T (1995) J Colloid Interface Sci 171:55–62
22. Baker JA, Henderson D (1967) J Chem Phys 47:2856
23. Wadachi M, Toda M (1972) J Phys Soc Jpn 32:1147
24. Hachisu S, Kobayashi Y, Kose A (1973) J Colloid Interface Sci 42:342
25. Brenner SL (1976) J Phys Chem 80:1473
26. Takano K, Hachisu S (1977) J Chem Phys 67:2604
27. Barnes CJ, Chan DY, Everett DH, Yates DE (1978) J Chem Soc Faraday Trans 2 74:136
28. Voeglli LP, Zukoski IV CF (1991) J Colloid Interface Sci 141:79
29. Okubo T (1994) Langmuir 10:1695–1702
30. Yerazuris S, Cornell SW, Winter B (1965) Nature 207:835
31. Sanders BJ, Murray MJ (1978) Nature 275:201
32. Sanders BJ (1980) Philos Mag 42:705
33. Sanders BJ, Murray MJ (1980) Philos Mag 42:721
34. Yoshimura S, Hachisu S (1980) Nature 283:188
35. Yoshimura S, Hachisu S (1985) J Phys (Paris) Colloq 46:C3–115
36. Hachisu S, Yoshimura S (1987) In: Safran SA, Clark NA (eds) Physics of complex and super-molecular fluids. Wiley, New York, p 221